Thermal and thermoelastic response of materials with thick-disk geometry excited by a ring-shaped laser beam

Michel Isidro-Ojeda, Jose Ordonez-Miranda, Luis Malacarne, Juan Alvarado-Gil

Thermal and thermoelastic response of materials with thick-disk geometry excited by a ring-shaped laser beam

Michel A. Isidro-Ojeda,[1, a)] Juan J. Alvarado-Gil,[1] Luis C. Malacarne,[2] and Jose Ordonez-Miranda[3]
[1)] *Departamento de Física Aplicada, Centro de Investigación y de Estudios Avanzados del I.P.N.-Unidad Mérida, Carretera Antigua a Progreso km. 6, A. P. 73 Cordemex, Mérida, Yucatán, 97310, Mexico*
[2)] *Departamento de Física, Universidade Estadual de Maringá, Av. Colombo 5790, 87020-900 Maringá PR, Brazil*
[3)] *Institut Pprime, CNRS, Université de Poitiers, ISAE-ENSMA, F-86962 Futuroscope Chasseneuil, France*

(Dated: 11 May 2020)

The heat and thermoelastic equations are analytically solved for a material with low optical absorption. This set of equations shows profiles describing the temperature distribution, surface displacement, stresses and optical path for a sample with a thick-disk geometry when is excited by a ring-shaped laser beam. This is done by determining the steady-state because when a laser beam is used, it turns on for several minutes to stabilize before using it in experiments. It is shown that the temperature takes some seconds to reach the steady-state condition, then, this approximation is very useful and simplifies the data processing. These results were also compared with a Gaussian profile, showing that the Gaussian equations are a consequence of the ring-shaped laser beam equations. The finite element method is used as a form of validation of the equations found in this work, obtaining a good agreement between numerical results. Errors are calculated for the temperature, displacement and optical path difference at the center(edge) of the sample; these are around 0.14 %(0 %), 0.11 %(30.50 %) and 0.09 %(4.86 %), respectively, for a BK7 sample. The analytical results obtained could be of great help in the design of the optical components and different experimental configurations. Maybe the principal advantage of a ring-shaped laser beam is to produce a temperature profile with a top-hat form at steady-state, while that a top-hat laser beam does not.

PACS numbers: Valid PACS appear here
Keywords: Ring-shaped, Photothermal effects, Thermal lensing

I. INTRODUCTION

Laser technology introduced new ideas for the design of experimental setups and photothermal spectroscopy is not an exception. This spectroscopic technique is based on the transformation of light into heat at the sample. And it has been used for materials characterization. So, the knowledge of the laser beams is crucial for the correct interpretation of the heat transfer through the materials. When a laser beam impinges a material, different effects occur. Gaussian laser beams have been widely used and characterized, also to being used in numerous experiments,[1–7] which has been used in various photothermal techniques for the characterization of materials. Research on other forms of distribution, such as the top-hat laser beam, has also been studied.[8,9] There is an excellent work describing the temperature profile for a ring-profile laser beam.[27] Many techniques are based on laser beam technologies in which the laser beam profile is very important for the correct description of the phenomena, some examples are thermal lens spectroscopy[10–14] and thermal mirror spectroscopy.[15–18] These have been used successfully in characterizing many materials. To improve the design of an experimental setup used in optical experiments using many lenses, mirrors and different optical components; it is necessary to know what happens to the instrumentation used, especially in experiments that include high-power laser beams; for example, when samples with very low optical absorption (water, alcohols, glasses, etc.) are explored. Optical path difference (OPD) is the basis of these methods. Analytical solutions to the complex thermoelastic problem have been approached using simplifications, these are known as thin-disk[19] or long-rod[5] approximations. A complete analysis for material with thick-disk geometry that is exposed to a Gaussian laser beam has been shown in a previous work.[20] The present study considers a ring-shaped laser beam, it should be mentioned that this type of laser beam can provide constant power at the center of a sample at steady-state.

The finite element method (FEM) has been used to predict how a system behaves in different situations.[21–25] For this reason, the FEM is an excellent complement to the theoretical analysis developed in this work. Using the equations obtained and the FEM, different numerical analyzes were performed and a good agreement was calculated between methods. Furthermore, our equations for a ring-shaped laser beam were compared with a Gaussian profile to observe the differences between temperature, displacement, stresses and OPD profiles.

[a)] michel.isidro15@gmail.com

To compare the results obtained, other models were used that have been used to describe the steady-state temperature profile. These models for a Gaussian[26] and ring-shaped[27] laser beam show a very good agreement with the results of this work for both the analytical model and the FEM. This gives the confidence to continue with the solution of the thermoelastic equation. Furthermore, these results obtained for a ring-shaped laser beam could be used for the determination of thermal and optical properties as has been done using different laser beams profiles.

The goal of this work is to provide analytical expressions to describe the temperature profile produced by a ring-shaped laser beam in a material with thick-disk geometry and the consequent deformation. And to obtain a more general expressions for laser beams at steady-state.

II. THEORETICAL MODEL

A. Temperature distribution

Fig. 1 shows that both the sample and laser beams can be described using a cylindrical coordinate system. This geometric configuration is very convenient considering that the sample has a thick-disk shape and that the laser beam profile is ring-shaped. So, the heat diffusion equation is given by

$$\frac{\partial \Delta T(r,z,t)}{\partial t} - D\nabla^2 \Delta T(r,z,t) = Q(r,z), \qquad (1)$$

where $\Delta T(r,z,t)$ is the temperature difference according to the radius r, thickness z and time t. $D = k/(\rho c)$ is the thermal diffusivity where k, ρ and c are the thermal conductivity, density and specific heat of the sample, respectively. $Q(r,z)$ is the t-independent heat source. $Q(r,z) = Q_0 f(r) e^{-A_e z}$, where[8,27,28]

$$Q_0 = \begin{cases} \frac{1}{2}\frac{Q_1}{\omega_e^2 - \omega_i^2} & \text{, for a ring-shaped laser beam} \\ \frac{Q_1}{\omega_G^2} & \text{, for a Gaussian laser beam} \end{cases}, \qquad (2)$$

where $Q_1 = 2AP_0(1-R)/(\pi c\rho)$. A is the optical absorption coefficient at the wavelength of the laser beam. P_0, ω_e and ω_i are the power, the external and the internal radius of the laser beam, respectively. ω_G is the radius of the Gaussian laser beam where its intensity decreases to $1/e^2$. R is the material's surface reflectivity. For optical systems with low optical absorption, the approximation $e^{-A_e z} \to 1$ can be used. Laser beam profile $f(r)$ is as follows

$$f(r) = \begin{cases} \theta(r-\omega_i)\theta(\omega_e - r) & \text{, for a ring-shaped beam} \\ e^{-2r^2/\omega_G^2} & \text{, for a Gaussian beam} \end{cases}, \qquad (3)$$

where θ is the Heaviside function. Hence, Eq. (1) is rewritten z-independent as

$$\frac{\partial \Delta T(r,t)}{\partial t} - D\frac{1}{r}\frac{\partial}{\partial r}\left(r\frac{\partial}{\partial r}\right)\Delta T(r,t) = Q(r). \qquad (4)$$

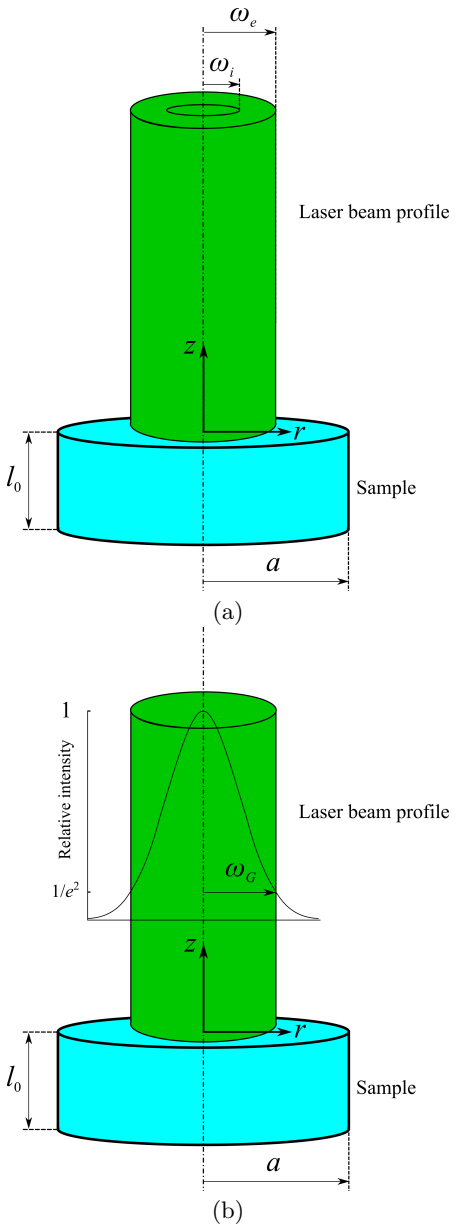

FIG. 1. Geometry of the laser beam profile and sample. This is important for the coordinates' system used in the solution of the heat and thermoelastic equations. (a) Ring-shaped laser beam: a, l_0 are the radius and thickness of the sample, respectively. ω_i and ω_e are the internal and external radius of the laser beam, respectively. (b) Gaussian laser beam: a, l_0 are the radius and thickness of the sample, respectively. ω_G is the radius of the Gaussian laser beam where its relative intensity is $1/e^2$.

Eq. (4) is subject to the boudary condition $\Delta T(a,t) = 0$ and the initial condition $\Delta T(r,0) = 0$. According to the method of separation of variables, the temperature distribution can be described by an infinite sum of zero-

order Bessel functions J_0, as follows

$$\Delta T(r,t) = \sum_{n=1}^{\infty} A_n(t) J_0\left(\alpha_n \frac{r}{a}\right), \tag{5}$$

where α_n are the zeros of J_0. To find $A_n(t)$, the laser beam must be represented similarly to $\Delta T(r,t)$, in order to do that, we write down

$$f(r) = \sum_{n=1}^{\infty} B_n J_0\left(\alpha_n \frac{r}{a}\right), \tag{6}$$

where B_n is found taking into account the orthogonality conditions. Therefore, we get the expressions for B_n as follows

$$B_{n,R} = \frac{1}{aJ_1^2(\alpha_n)} \left\{ \frac{2}{\alpha_n} \left[\omega_e J_1\left(\frac{\alpha_n \omega_e}{a}\right) - \omega_i J_1\left(\frac{\alpha_n \omega_i}{a}\right) \right] \right\} \tag{7a}$$

and

$$B_{n,G} = \frac{1}{aJ_1^2(\alpha_n)} \frac{\omega_G^2}{2a} e^{-\frac{1}{2}\left(\frac{\alpha_n \omega_G}{2a}\right)^2}, \tag{7b}$$

for a ring-shaped and Gaussian laser beam, respectively. By replacing one of Eqs. (7) in Eq. (6), the laser beam profile is obtained in terms of a sum of first-order Bessel functions J_1. It can be seen in Eq. (7a) that when $\omega_e = \omega_i$ the value of $B_{n,R}$ is equal to zero, this means that there is no heat source as expected. When $\omega_i = 0$ and taking into account that $\omega_{e,G} \leq a$, then $B_{n,R} = 2B_{n,G}$. This last result suggests that $Q(r)$ for a Gaussian profile is a consequence of ring-shaped $Q(r)$ at steady-state and when $l_0 \ll a$. Substituting Eq. (5) and Eq. (6) in the heat diffusion equation given by Eq. (4), we have the next differential equation

$$\frac{d}{dt} A_n(t) + \frac{D\alpha_n^2}{a^2} A_n(t) - B_n Q_0 = 0, \tag{8}$$

whose solution is given by

$$A_n(t) = B_n Q_0 \frac{a^2}{D\alpha_n^2} \left(1 - e^{-\frac{t}{\tau}\alpha_n^2}\right), \tag{9}$$

where $\tau = a^2/D$ is the thermal diffusion time and B_n is given by Eqs. (7). Eq. (9) is very important because it describes the shape and behavior of the laser beam. Where the second term (in parentheses) contains the time dependency, where it can be seen that when $t \to \infty$ this term is equal to 1, this way the steady-state is obtained. This last approach is very important in practice because laser beams need stabilization before using them in experiments. Substituting Eq. (9) in Eq. (5), with B_n given by Eq. (7a), we have an equation that describes the temperature profile when a ring-shaped laser beam excites a sample. This equation matches very well the set of equations (3) found by Kim *et al.*[27]

B. Thermoelastic equation

Heating produces a deformation in the sample. For this reason, it is important to understand the thermoelastic behavior that said heat produces. It is called thermoelasticity because the deformation of the structure does not exceed the elastic limit and when the heat source disappears the deformation also does.[29] Thermoelasticity theory makes possible to calculate the stresses in a body produced by a temperature field. This theory includes heat conduction, strains and stresses due to a heat source.[30] As has been shown in a previous work,[20] the displacement vector (u_i) and the stress components (σ_{ij}) are obtained from

$$\begin{aligned} u_i(r,z,t) =& \partial_i \Psi(r,z,t) \\ &+ \frac{1}{1-2\nu} \left[2(1-\nu)\delta_{zi}\nabla^2 - \partial_{zi} \right] \psi(r,z,t) \end{aligned} \tag{10}$$

and

$$\begin{aligned} \sigma_{ij}(r,z,t) =& 2\mu \left(\partial_{ij} - \delta_{ij}\nabla^2\right) \Psi(r,z,t) \\ &+ \frac{2\mu}{1-2\nu} \left[\partial_z \left(\nu \delta_{ij} \nabla^2 - \partial_{ij} \right) \right. \\ &\left. + (1-\nu)\nabla^2 \left(\delta_{iz}\partial_j + \delta_{jz}\partial_i \right) \right] \psi(r,z,t), \end{aligned} \tag{11}$$

where ∇^2 is the Laplacian operator, δ_{ij} is the the Kronecker delta function. $\mu = Y/[2(1+\nu)]$ where ν is the Poisson ratio and Y is the Young's modulus of the sample. Using the thermoelastic displacement potential Ψ and Love function ψ, the thermoelastic equation can be expressed by

$$\nabla^2 \Psi(r,t) = m \Delta T(r,t) \tag{12}$$

and

$$\nabla^2 \nabla^2 \psi(r,z,t) = 0. \tag{13}$$

Eqs. (12) and (13) are known as the Poisson and Love equations, respectively. $m = \alpha_T(1+\nu)/(1-\nu)$, where α_T is the linear thermal expansion coefficient.
Using Eq. (5), solutions of (12) and (13) take the following form

$$\Psi(r,t) = -\sum_{n=1}^{\infty} \frac{ma^2}{\alpha_n^2} A_n(t) J_0\left(\frac{\alpha_n r}{a}\right) \tag{14}$$

and

$$\begin{aligned} \psi(r,z,t) = \sum_{n=1}^{\infty} \frac{J_0\left(\frac{\alpha_n r}{a}\right)}{(\alpha_n/a)^2} \left[\left(B_1 + B_2 \frac{\alpha_n}{a} z \right) e^{\alpha_n z/a} \right. \\ \left. + \left(C_1 + C_2 \frac{\alpha_n}{a} z \right) e^{-\alpha_n z/a} \right], \end{aligned} \tag{15}$$

respectively. The solutions for the constants B_1, B_2, C_1 and C_2 can be consulted in the reference,[20] when $\sigma_{zz} =$

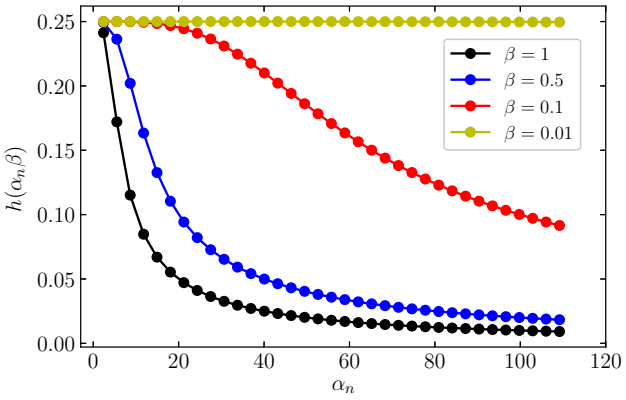

FIG. 2. Behavior of $h(\alpha_n\beta)$ for $J_0(\alpha_n) = 0$, $n = 1, ..., 35$. It can be seen that when $h(\beta \to 0) = 1/4$, this means the thin-disk approximation ($l \ll a$).

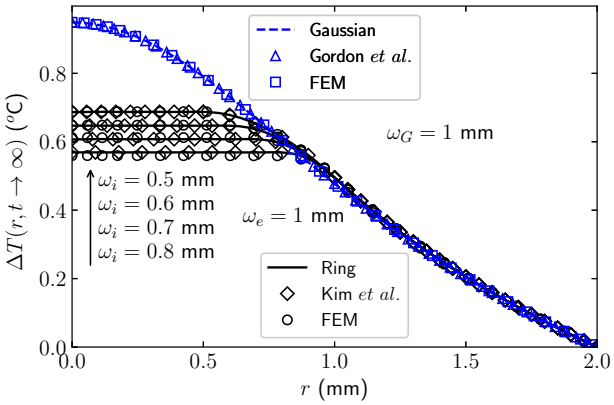

FIG. 3. Temperature profile created by a ring-shaped laser beam varying the internal radius ω_i with a constant external radius ω_e. ω_G is the radius for a Gaussian laser beam. All these data were created at steady-state, this means $t \to \infty$.

$\sigma_{rz} = 0$ at $z = 0$ and $z = l_0$. To account for edge deformation for a thick-disk material, it is necessary to use[30]

$$u_z \to u_z + 2N\frac{\nu\,(z - l_0/2)}{Y}, \tag{16}$$

$$\sigma_{rr} \to \sigma_{rr} - N \quad \text{and} \quad \sigma_{\phi\phi} \to \sigma_{\phi\phi} - N. \tag{17}$$

Then, the displacement on the faces of the sample can be expressed as

$$\begin{aligned} u_z(r, 0, t) &= -u_z(r, l_0, t) \\ &= \sum_{n=1}^{\infty} \frac{A_n(t)\alpha_T}{\alpha_n}\left[-2\alpha_n h(\alpha_n) l_0\,(\nu + 1)\,J_0\left(\frac{\alpha_n r}{a}\right)\right. \\ &\left. + \frac{l_0 \nu J_1\,(\alpha_n)}{\nu - 1}\,(4h(\alpha_n)\nu - 1)\right] \end{aligned} \tag{18}$$

with

$$h(\alpha_n\beta) \equiv \frac{\cosh\,(\alpha_n\beta) - 1}{\alpha_n\beta\,[\sinh\,(\alpha_n\beta) + \alpha_n\beta]}, \tag{19}$$

where $\beta = l_0/a$.

Fig. 2 shows the behavior of Eq. (19) for the first thirty-five α_n values that produce $J_0(\alpha_n) = 0$. It can be seen that when $\beta \to 0$ it is obtained that $h(\alpha_n\beta) = 1/4$, this means that the thin-disk approximation is reached. Now, using the general equations for the OPD shown in a previous work[20] and equations found here, we have a complete set of equations for the correct description of the OPD when a laser beam heats a material with thick-disk configuration.

III. RESULTS AND DISCUSSION

Fig. 3 shows the temperature distribution produced by a ring-shaped laser beam and one with a Gaussian profile. Data used for the calculus can be found in a previous work[20] for a BK7 sample. It can be seen a very good agreement between Eq. (5) with $A_n(t)$ given by Eq. (9) and B_n given by Eq. (7a), found in this work and represented by continuous lines, and Eqs. (3) reported by Kim *et al.*[27] represented by diamonds. It is shown how the temperature profile changes as a function of ω_i. The value of ω_e is kept constant. When ω_i becomes zero, it gives a top-hat profile. In the same figure, the result of a Gaussian laser beam (Eq. (5) with Eq. (9) and Eq. (7b)), found in a previous work is shown represented by the dashed line.[20] The latter is compared with the equation found by Gordon *et al.*,[26] represented by triangles, also obtaining a very good agreement. It is important to mention that these curves were obtained at steady-state, this means that $t \to \infty$. The FEM was used to validate the theoretical model proposed in this work. Circles and squares are for ring and Gaussian FEM simulations.

Fig. 4 shows the temperature dependence as a function of r and ω_i for the x-axis and y-axis, respectively. The outer radius for the ring-shaped laser beam was set at $\omega_e = 1$ mm. It can be seen that for $r = \omega_e$ the value of ΔT decreases independently of the value given for the internal radius ω_i. Furthermore, the behavior of the decrease of ΔT is the same after that value of $r = \omega_e$. It is important to say that when the $\omega_i = \omega_e$ there is no representation because there is no laser beam.

In Fig. 5 is shown the temperature distribution in a sample for (a) a ring-shaped and (b) a Gaussian laser beam. These were generated using the models found in this and a previous work.[20] These graphs allow observing how the sample is affected by the incidence of a ring-shaped and a Gaussian laser beam. Furthermore, in the models, these calculations can be carried out as a function of time, then the behavior of the sample since the laser beam is applied on the sample can be recorded until it reaches the steady-state.

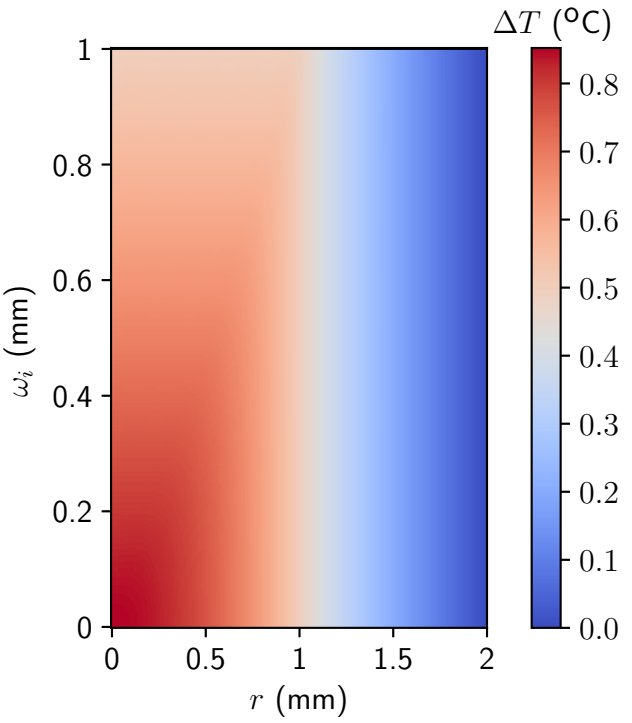

FIG. 4. Temperature difference, ΔT, as a function of r (x-axis) and ω_i (y-axis). The value of ω_e is set at 1 mm. Also, $a = l_0 = 2$ mm.

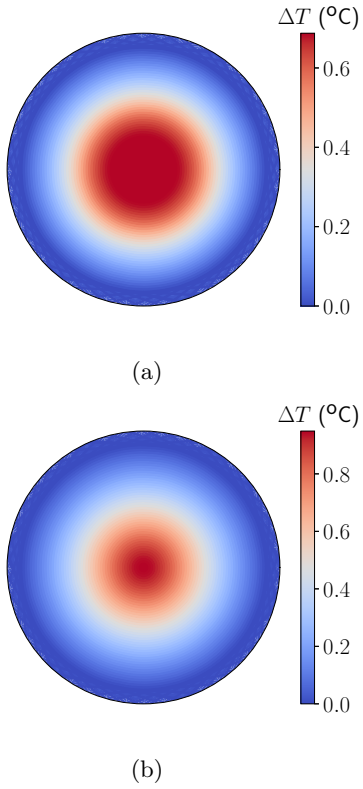

FIG. 5. Temperature distribution generated with the (a) ring-shaped and (b) Gaussian model.

Fig. 6 shows the displacement calculations using Eq. (18). The FEM was used as a validation method, and we can see that there is a good agreement between both methods. In addition, a comparison with the Gaussian model is shown. For the ring model, $\omega_e = 1$ mm is maintained, while the value of ω_i takes the values 0.8, 0.7, 0.6 and 0.5 mm. It can be seen that when the internal radius goes to zero, the maximum value of u_z increases until reaching a behavior similar to that of a Gaussian laser beam.

Figs. 7 and 8 show the radial and angular stress along the z-axis, respectively. It can be seen that the absolute maximum value is presented in the middle of the sample, this means at $z = l_0/2$. As ω_i goes to zero, the absolute maximum value increases. It should be noted that when $\omega_i \to 0$, the data for the ring-shaped laser beam takes the form of σ_{rr} and $\sigma_{\phi\phi}$ for a Gaussian laser beam.

The stress along the z-axis for σ_{zz} is presented in Fig. 9. It can be seen how σ_{zz} goes from positive to negative values at the center of the sample as the internal radius is decreasing. The data shown correspond to $\omega_i = 0.8, 0.7, 0.6$ and 0.5 mm keeping the value of $\omega_e = 1$ mm as was done previously.

Fig. 10 shows total OPD in a sample with $l_0 = a = 2$ mm. It can be observed how at the center of the graph it is shaped like a top-hat when a ring-shaped laser beam is used to heat. The fall of the curve that represents the

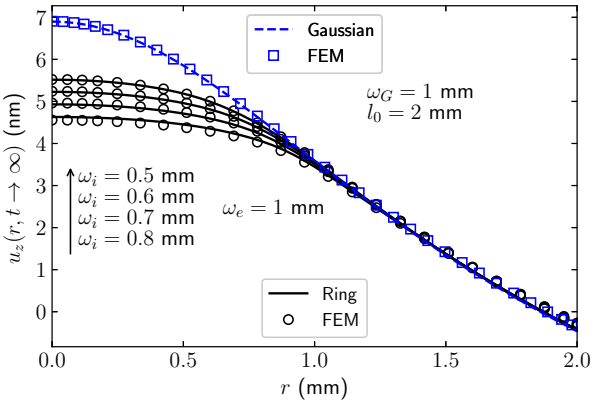

FIG. 6. Displacement presented in a sample with thick-disk geometry, using $l_0 = r = 2$ mm. A comparison between ring and Gaussian model is shown. It can be seen that when $\omega_i \to 0$, the ring model tends to the same behaviour as that of a Gaussian laser beam.

ΔS appears in the internal radius of the laser beam, that is, in the value of ω_i. Remember that these data were calculated using the steady-state.

To appreciate how the value of ΔS increases with time, different calculations were performed, which are shown in Fig. 11. These calculations were made at the center of

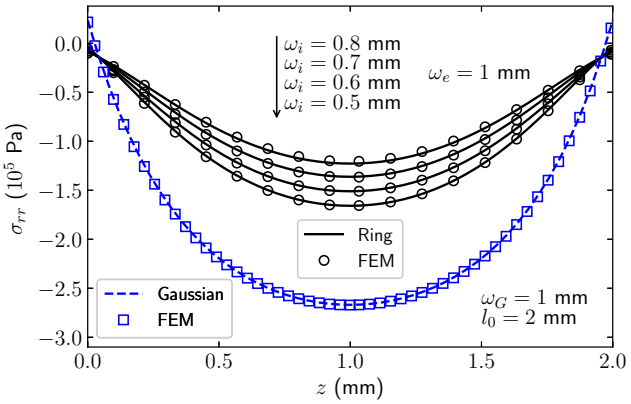

FIG. 7. Radial stress for a material with thick-disk geometry at $r = 0$ by using a ring-shaped laser beam. The sample has the dimensions $l_0 = a = 2$ mm. It is shown a comparison with the FEM and the model that describes a Gaussian laser beam.

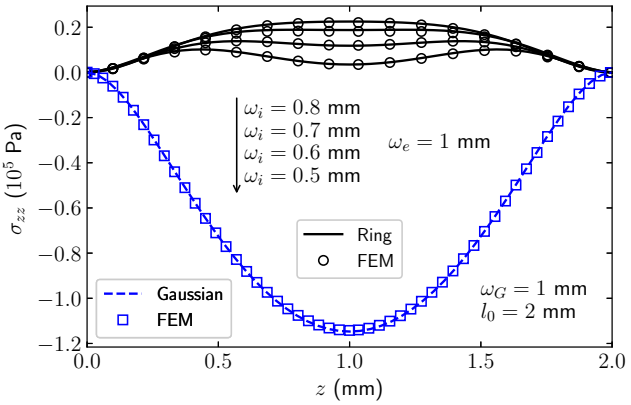

FIG. 9. Stresses along the z-axis are shown when a ring-shaped laser beam at $r = 0$ is used. It can be seen how the behavior of the graph goes from positive values to negative values when ω_i is decreasing. The absolute maximum value is obtained when $\omega_i = 0$, recovering the data for a Gaussian laser beam with $\omega_G = 1$ mm as can be seen.

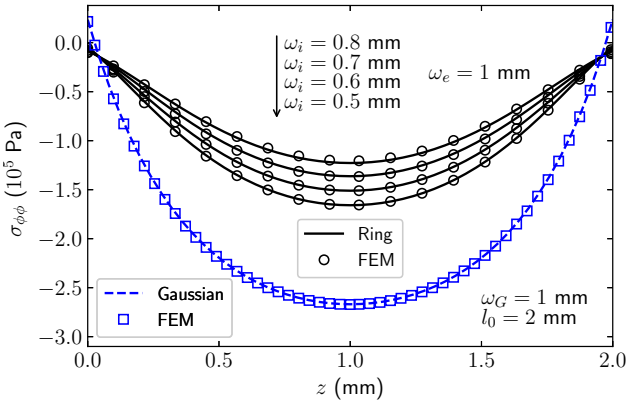

FIG. 8. Angular stress for a material with thick-disk geometry at $r = 0$ by using a ring-shaped laser beam. The sample has the dimensions $l_0 = a = 2$ mm. It is shown a comparison with the FEM and the model that describes a Gaussian laser beam.

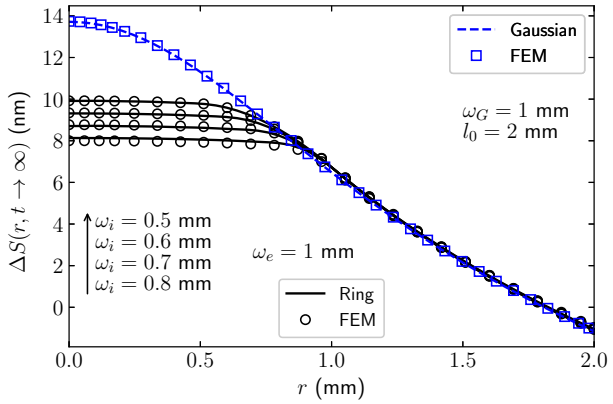

FIG. 10. Total OPD for material with thick-disk geometry by using a ring-shaped laser beam. The FEM and the model describing a Gaussian laser beam were used to compare results.

the sample, this means when $r = 0$. As can be seen in the figure, ΔS does not rise instantaneously for the ring-shaped laser beam, observe continuous lines, this makes sense because at the center of this type of laser beam, there is no heat source. This does not happen for a Gaussian laser beam as can be seen in the same figure, where it can be seen that the increase of ΔS is instantaneous, observe dashed lines. Furthermore, it can be seen that at $t = 5$ seconds, the value of the total OPD is almost constant, for this reason, a steady-state approximation can be used successfully for the data calculations when studying low absorption samples with thick-disk geometry by using a ring-shaped laser beam.

IV. CONCLUSIONS

We have solved the heat diffusion and thermoelastic equation for a laser beam with a ring profile. We have shown some differences concerning the profile of the Gaussian laser beam. In both cases, we have used the FEM as a validation method, and we have obtained very good results. Expressions that have been found are more general for the description of a laser beam, going from a ring-shaped to a Gaussian-shape at steady-state. We have calculated the percentage differences between expressions found and FEM for the temperature, displacement and optical path difference at the center(edge) of the sample; these are approximately 0.14 % (0 %), 0.11 % (30.50 %) and 0.09 % (4.86 %), respectively. The ad-

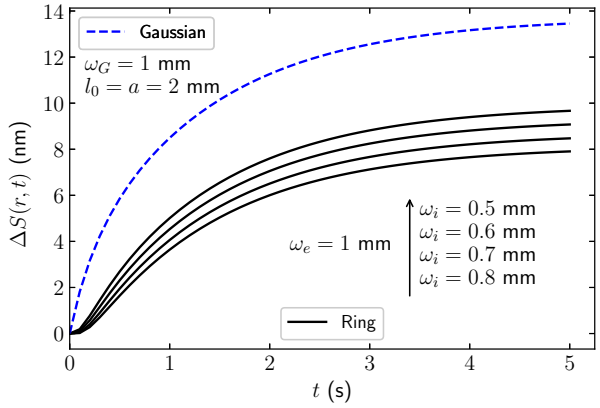

FIG. 11. OPD time-resolved for the first 5 seconds at the center of material with thick-disk geometry.

vantage of a ring-shaped laser beam over the Gaussian laser beam is that the former shows a homogeneous circular temperature distribution at steady-state, which is known as a top-hat distribution. These calculations can be used in the design of optical instrumentation and the characterization of low absorption samples with thick-disk geometry when a laser beam with a ring profile is used.

REFERENCES

[1] C. A. Klein, "Describing beam-aberration effects induced by laser-light transmitting components: a short account of raytheon's contribution," Laser Weapons Technology II **4376**, 24 (2001).

[2] W. Winkler, K. Danzmann, A. Rüdiger, and R. Schilling, "Heating by optical absorption and the performance of interferometric gravitational-wave detectors," Physical Review A **44**, 7022 (1991).

[3] M. Sparks, "Optical distortion by heated windows in high-power laser systems," Journal of Applied Physics **42**, 5029 (1971).

[4] M. Mansuripur and C. Pons, "Diffraction modeling of optical path for magneto-optical disk systems," Optical Storage Technology and Applications **899**, 56 (1988).

[5] C. A. Klein, "Optical distortion coefficients of high-power laser windows," Optical Engineering **29**, 343 (1990).

[6] Y. Peng, Z. Sheng, H. Zhang, and X. Fan, "Influence of thermal deformations of the output windows of high-power laser systems on beam characteristics," Applied optics **43**, 6465 (2004).

[7] C. A. Klein, "Analytical stress modeling of high-energy laser windows: application to fusion-cast calcium fluoride windows," Journal of applied physics **98**, 043103 (2005).

[8] N. G. Astrath, F. B. Astrath, J. Shen, J. Zhou, P. R. Pedreira, L. C. Malacarne, A. C. Bento, and M. L. Baesso, "Top-hat cw-laser-induced time-resolved mode-mismatched thermal lens spectroscopy for quantitative analysis of low-absorption materials," Optics letters **33**, 1464 (2008).

[9] C. Zhao, J. Degallaix, L. Ju, Y. Fan, D. G. Blair, B. J. J. Slagmolen, M. B. Gray, C. M. Lowry, D. McClelland, D. Hosken, *et al.*, "Compensation of strong thermal lensing in high-optical-power cavities," Physical review letters **96**, 231101 (2006).

[10] J. Shen, M. L. Baesso, and R. D. Snook, "Three-dimensional model for cw laser-induced mode-mismatched dual-beam thermal lens spectrometry and time-resolved measurements of thin-film samples," Journal of applied physics **75**, 3738 (1994).

[11] S. Luterotti, M. Sikovec, and D. Bicanic, "Ultrasensitive determination of trans-β-carotene in rat and beef livers by means of high-performance liquid chromatography coupled with thermal lens detection," Talanta **53**, 103 (2000).

[12] M. Franko and C. D. Tran, "Analytical thermal lens instrumentation," Review of scientific instruments **67**, 1 (1996).

[13] M. Franko, P. van de Bovenkamp, and D. Bicanic, "Determination of trans-β-carotene and other carotenoids in blood plasma using high-performance liquid chromatography and thermal lens detection," Journal of Chromatography B: Biomedical Sciences and Applications **718**, 47 (1998).

[14] N. Astrath, J. Rohling, A. Medina, A. Bento, M. Baesso, C. Jacinto, T. Catunda, S. Lima, F. Gandra, M. Bell, *et al.*, "Time-resolved thermal lens measurements of the thermo-optical properties of glasses at low temperature down to 20 k," Physical Review B **71**, 214202 (2005).

[15] N. Astrath, L. Malacarne, P. Pedreira, A. Bento, M. Baesso, and J. Shen, "Time-resolved thermal mirror for nanoscale surface displacement detection in low absorbing solids," Applied Physics Letters **91**, 191908 (2007).

[16] L. Malacarne, F. Sato, P. Pedreira, A. Bento, R. Mendes, M. Baesso, N. Astrath, and J. Shen, "Nanoscale surface displacement detection in high absorbing solids by time-resolved thermal mirror," Applied physics letters **92**, 131903 (2008).

[17] V. Zanuto, L. Herculano, M. Baesso, G. Lukasievicz, C. Jacinto, L. Malacarne, and N. Astrath, "Thermal mirror spectrometry: An experimental investigation of optical glasses," Optical Materials **35**, 1129 (2013).

[18] G. Bianchi, V. Zanuto, F. Astrath, L. Malacarne, I. Terra, T. Catunda, L. A. d. O. Nunes, C. Jacinto, L. Andrade, S. Lima, *et al.*, "Resonant excited state absorption and relaxation mechanisms in tb 3+-doped calcium aluminosilicate glasses: an investigation by thermal mirror spectroscopy," Optics letters **38**, 4667 (2013).

[19] G. Zhu, X. Zhu, Z. Dai, Z. Wang, and C. Zhu, "Analytical model of optical path difference in an end-pumped yb: Yag thin-disk laser with nonuniform pumping light," Applied optics **54**, 3024 (2015).

[20] M. A. Isidro-Ojeda, J. J. Alvarado-Gil, V. S. Zanuto, M. L. Baesso, N. G. Astrath, and L. C. Malacarne, "Laser induced wavefront distortion in thick-disk material: An analytical description," Optical Materials **75**, 574 (2018).

[21] V. Sazegari, M. R. J. Milani, and A. K. Jafari, "Structural and optical behavior due to thermal effects in end-pumped yb: Yag disk lasers," Applied optics **49**, 6910 (2010).

[22] M. J. Milani, V. Sazegari, and A. K. Jafari, "Calculating optical path difference in end-pumped yb: Yag thin disk lasers," 16th International School on Quantum Electronics: Laser Physics and Applications **7747**, 774718 (2011).

[23] G. Zhu, X. Zhu, M. Wang, Y. Feng, and C. Zhu, "Analytical model of thermal effect and optical path difference in end-pumped yb: Yag thin disk laser," Applied optics **53**, 6756 (2014).

[24] H. Aminpour and C. Pflaum, "Optical path difference of slanted edge diode-pumped yb: Yag/yag thin-disk laser," (International Society for Optics and Photonics, 2014) p. 89591V.

[25] R. Anufriev, J. Ordonez-Miranda, and M. Nomura, "Measurement of the phonon mean free path spectrum in silicon membranes at different temperatures using arrays of nanoslits," Physical Review B **101**, 115301 (2020).

[26] J. Gordon, R. Leite, R. Moore, S. Porto, and J. Whinnery, "Long-transient effects in lasers with inserted liquid samples," Journal of Applied Physics **36**, 3 (1965).

[27] D. Kim, S. Noh, S. Ahn, and J. Kim, "Influence of a ring-shaped pump beam on temperature distribution and thermal lensing in end-pumped solid state lasers," Optics Express **25**, 14668 (2017).

[28] L. C. Malacarne, N. G. Astrath, and M. L. Baesso, "Unified theoretical model for calculating laser-induced wavefront distortion in optical materials," JOSA B **29**, 1772–1777 (2012).

[29]S. Timoshenko and J. Goodier, "Theory of elasticity, by s. timoshenko and j.n. goodier, ... 2nd edition," (1951).

[30]W. Nowacki, "Thermoelasticity, by w. nowacki," International Series of Monographs on Aeronautics and Astronautics. Division I: Solid and Structural Mechanics, V.3 (1962).